Analysis of Envelope Signal Injection for Improvement of RF Amplifier Intermodulation Distortion

Vincent W. Leung, Junxiong Deng, Prasad S. Gudem and Lawrence E. Larson

Center for Wireless Communication
University of California, San Diego
La Jolla, CA 92093, USA

Abstract

Adaptive bias techniques based on envelope signal power detection have been proposed for linearity enhancement and dc current reduction in RF amplifiers [1-2]. Experimental results show an improvement in amplifier linearity, although asymmetric intermodulation distortion (IMD) was observed. This paper studies the effects of the magnitude and phase of the envelope signal injection on amplifier linearity, and illustrates a technique in which the IMD can be optimally cancelled.

I. Introduction

In order to accommodate high data-rate transmission for third generation (3G) wireless communications, spectrally-efficient variable envelope modulation schemes are employed. The hybrid phase-shift keying (HPSK) adopted for the wideband CDMA (WCDMA) standard is one example [3]. Spectral regrowth due to transmitter circuit distortion must be strictly limited; this often translates to stringent and challenging linearity requirements for the transmitter chain radio frequency (RF) amplifiers. Another important, although often conflicting, design criterion is minimizing the amplifier power consumption. Since RF amplifiers consume a significant share of the battery power in a mobile device, their power efficiencies have a direct and determining impact on the talk time. Further complicating the issue, not only should the efficiency be maximized at the peak power level (without compromising the amplifier linearity), it should also be kept high during the power backoff mode.

As a result, the amplifier should exhibit high *average* efficiency to prolong battery life. The amplifier's bias should be adaptive; for small-signal conditions, the quiescent current should be kept to its minimum to enhance the efficiency. For large-signal conditions, the current should automatically rise so that high linearity is achieved.

With these design criteria in mind, adaptive-biased RF amplifiers were recently proposed [1-2]. The underlying concept is shown in Figure 1. A rise in the input power causes a proportional rise in the bias current of the amplifier (where an envelope signal is superimposed), and results in improved linearity. The linearity enhancement with this technique will be examined, and optimum design criteria established.

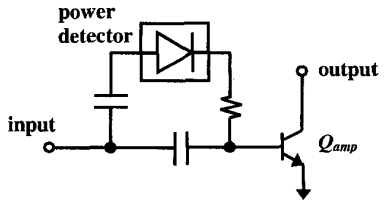

Figure 1. Conceptual diagram of the adaptive-bias RF amplifier. The power detector adjusts the dc bias in response to the input power

II. Linearity Analysis of Envelope Injection Technique

Power detection is accomplished by two bipolar devices (Q_1, Q_2) configured as common-emitter amplifiers, as shown in Fig. 2 [1]. They are biased with low quiescent current (I_o), so that their collector currents will be "clipped" during large-signal conditions. As a result, their average (dc) collector currents will be raised above the quiescent level. The extra dc current, which is proportional to the input power, will be mirrored to the input device of the RF amplifier.

On top of the dc current, the adaptive bias control circuit also produces an envelope current proportional to the signal power. Assuming a two-tone sinusoidal input at frequencies ω_1 and ω_2, the envelope signal is given by

$$i_{env}(t) = I_{env}\cos[(\omega_2 - \omega_1)t + \theta_{env}] \quad (1)$$

where I_{env} and θ_{env} denote the amplitude and the phase of the

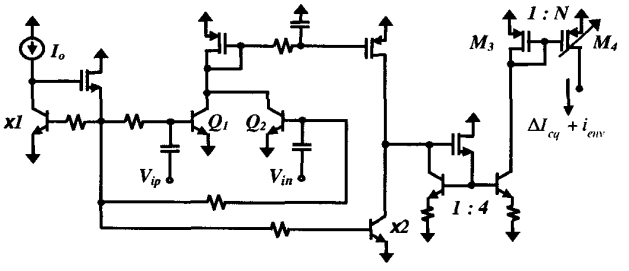

Figure 2. Power detector bias control circuit [1]. It provides a dc and an envelope signal component proportional to the input power.

envelope signal respectively. As such, the bias current of the amplifier transistor (the Q_{amp} shown in Figure 1), as well as its transconductance, are time-varying. For intermodulation calculations, this is modeled as an additional small-signal envelope signal voltage along with the two-tone RF inputs.

Volterra analysis is used to capture the frequency dependent nonlinearities, which dominate at high frequencies [4]. The equivalent nonlinear circuit is shown in Figure 3, where Z_S, Z_E and Z_L denote the source, emitter, and load impedances respectively. In this model, capacitance C_π and transconductance g_m are assumed to be the only nonlinear elements [5]. The i-v relationship of C_π is given by

$$i = \frac{d}{dt}[\, C_\pi v_{be} + K_{2C} v_{be}^2 + K_{3C} v_{be}^3 \,] \tag{2}$$

where K_{2C} and K_{3C} are the 2nd- and 3rd-order nonlinear capacitance coefficients, and v_{be} is the base-emitter voltage. Similarly, the nonlinear collector current is given by

$$i_c = g_m v_{be} + K_{2gm} v_{be}^2 + K_{3gm} v_{be}^3 \tag{3}$$

where K_{2gm} and K_{3gm} are the 2nd- and 3rd-order nonlinear transconductance coefficients. These coefficients are extracted from simulations of the bipolar transistor biased in the actual operating conditions. They will be employed to calculate the value of the nonlinear current sources $\tilde{i}_{N,C,\omega}$ and $\tilde{i}_{N,gm,\omega}$, which denote the N^{th}-order nonlinear capacitance and transconductance currents at frequency ω.

In our three-tone intermodulation test, where two input frequencies are at ω_1, and ω_2, and the third (envelope) signal input is at $\omega_3 = \omega_2 - \omega_1$, we will derive the resulting distortion using the method of nonlinear currents [4]. From Figure 3, by ignoring the nonlinear current sources, the fundamental collector and base-emitter voltages (at ω) are given by:

$$v_c(\omega) = \frac{[\, -g_m + j\omega C_\mu (1 + g_m Z_E) - \omega^2 C_\pi C_\mu Z_E \,] Z_L}{D(\omega)} v_s(\omega) \tag{4}$$

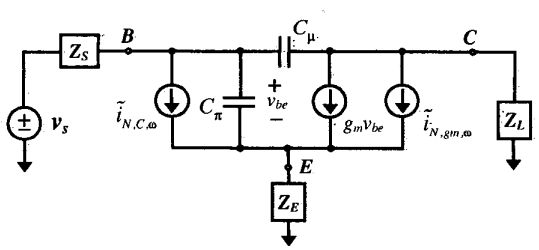

Figure 3. Nonlinear amplifier model, for Volterra analysis using method of nonlinear currents [4]. The fundamental signals are found by setting the nonlinear current sources to zero, while higher-order distortion voltages are evaluated by setting the signal source to zero.

$$v_{be}(\omega) = \frac{1 + j\omega C_\mu Z_L}{D(\omega)} v_s(\omega) \tag{5}$$

where $D(\omega)$ is given in the Appendix.

The 2nd-order base-emitter voltage at frequency ω is found to be

$$v_{be}(\omega) = -\{\, \tilde{i}_{2,gm,\omega}[\, Z_E + j\omega C_\mu (\, Z_L Z_S + Z_E Z_L + Z_S Z_E \,)] + \tilde{i}_{2,C,\omega}[\, Z_S + Z_E + j\omega C_\mu (\, Z_L Z_S + Z_E Z_L + Z_S Z_E \,)]\} / D(\omega) \tag{6}$$

For double frequency terms (such as $2\omega_1$), the nonlinear currents are given by [4]

$$\tilde{i}_{2,gm,2\omega} = \frac{K_{2gm}}{2} v_{be}^2(\omega) \qquad \tilde{i}_{2,C,2\omega} = K_{2C} j2\omega v_{be}^2(\omega) \tag{7}$$

Similarly, for difference frequency terms (such as $\omega_2 - \omega_1$), the nonlinear currents are given by

$$\begin{aligned} \tilde{i}_{2,gm,\omega_a-\omega_b} &= K_{2gm} v_{be}(-\omega_b) v_{be}(\omega_a) \\ \tilde{i}_{2,C,\omega_a-\omega_b} &= K_{2C} j(\omega_a - \omega_b) v_{be}(-\omega_b) v_{be}(\omega_a) \end{aligned} \tag{8}$$

The 3rd-order collector voltages can be written as:

$$\begin{aligned} v_c(\omega) = Z_L\{ &-\tilde{i}_{3,C,\omega}[\, -j\omega C_\mu Z_S + g_m (\, Z_E + Z_S \,)] \\ &-\tilde{i}_{3,gm,\omega}[\, 1 + j\omega C_\mu Z_S + j\omega C_\pi (\, Z_E + Z_S \,)]\} / D(\omega) \end{aligned} \tag{9}$$

The third-order IMD (IMD_3) currents are given by:

$$\begin{aligned} \tilde{i}_{3,gm,2\omega_a-\omega_b} &= K_{2gm}[\, ①+②+③+④ \,] + \frac{3K_{3gm}}{4}[\, ⑤+⑥ \,] \\ \tilde{i}_{3,C,2\omega_a-\omega_b} &= j(2\omega_a - \omega_b)\{ K_{2C}[\, ①+②+③+④ \,] + \frac{3K_{3C}}{4}[\, ⑤+⑥ \,]\} \end{aligned} \tag{10}$$

where ①-⑥ denote all possible combinations of the lower-order (fundamental and 2nd-order) terms that will give rise to the IMD_3 products. Specifically, for IMD_3 at $2\omega_1 - \omega_2$, these six terms are:

$$\begin{aligned} ① &= v_{be}(2\omega_1) v_{be}(-\omega_2) & ② &= v_{be}(\omega_2) v_{be}(-2\omega_3) \\ ③ &= v_{be}(\omega_1) v_{be}(\omega_1 - \omega_2) & ④ &= v_{be}(\omega_1) v_{be}(-\omega_3) \\ ⑤ &= v_{be}(-\omega_2) v_{be}^2(\omega_1) & ⑥ &= v_{be}(\omega_2) v_{be}^2(-\omega_3) \end{aligned} \tag{11}$$

By the same token, the corresponding products for the IMD_3 at $2\omega_2 - \omega_1$ are

$$\begin{aligned} ❶ &= v_{be}(-\omega_1) v_{be}(2\omega_2) & ❷ &= v_{be}(\omega_1) v_{be}(2\omega_3) \\ ❸ &= v_{be}(\omega_2) v_{be}(\omega_2 - \omega_1) & ❹ &= v_{be}(\omega_2) v_{be}(\omega_3) \\ ❺ &= v_{be}(-\omega_1) v_{be}^2(\omega_2) & ❻ &= v_{be}(\omega_1) v_{be}^2(\omega_3) \end{aligned} \tag{12}$$

Finally, the 3rd-order intermodulation ratio (IMR_3) is determined by the ratio between the fundamental and the third-order v_c given by (5) and (9).

Notice that the products denoted by ①③⑤ are the conventional IMD_3 components, as they are envelope signal (ω_1) independent. Among the remaining envelope-dependent terms, only ④ is of interest as the other two (②⑥) involve "squaring" the already small envelope input, and can be safely ignored.

The theoretical analysis leads to an intuitive understanding of the nonlinear behavior, as well as a strategy for high-linearity high-efficiency RF amplifier design, as will be explained below.

Since the envelope-dependent mixing products ④ and ❹ will typically have different phase relationships with the conventional distortion components, their summation can result in unequal IMD_3 amplitudes at $2\omega_1 - \omega_2$ and $2\omega_2 - \omega_1$. This scenario is graphically demonstrated in Figure 4, where the nonlinear current components are represented by vectors to highlight their interactions. In this example, the angle between vectors ❹ and Σ [❶❸❺] is less than that between ④ and Σ [①③④] (i.e., $\theta_1 < \theta_2$). As a result, their resultant vectors will exhibit different magnitudes. So, the IMD_3 at $2\omega_2 - \omega_1$ will be higher than that at $2\omega_1 - \omega_2$. It shows that asymmetric spectral regrowth is possible although the individual distortion components are equal in magnitude at both frequencies.

The vector diagram also points to the fact that if the injected envelope signal is too strong, vectors ④ and ❹ will dominate the final IMD_3 resultant vector, which is highly undesirable.

This also leads to a method for IMD_3 cancellation. It is straightforward to show that if the envelope signal is phase-shifted (with respect to the input RF signals), vectors ④ and ❹ will always rotate in opposite direction by the same angle: if one moves clockwise, the other will travel counter-clockwise. If these vectors can be simultaneously rotated to

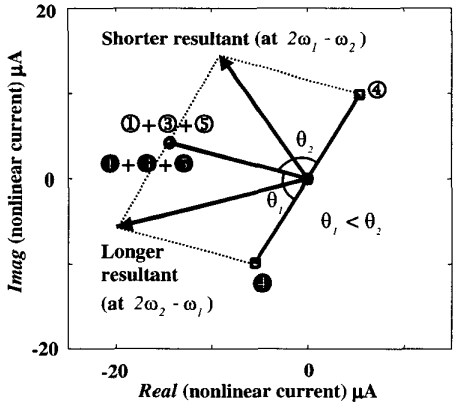

Figure 4. Vector diagram illustrating the cause of IMD_3 asymmetry. Vectors ④ and ❹ represent the injected envelope signal. Note that the two resulting IMD vectors will have different amplitudes depending on the phase of the envelope.

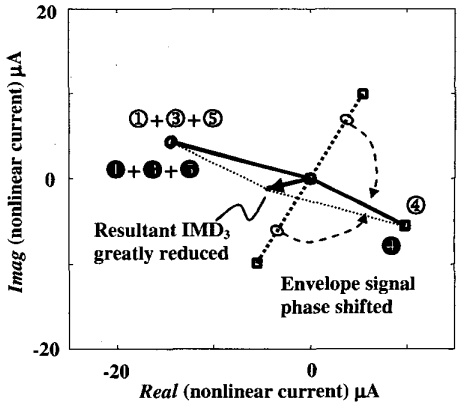

Figure 5. Vector diagram showing optimal IMD3 cancellation. Note that the injected envelope signal cancels the third-order components when its phase and amplitude are optimized.

be at 180° opposite to the vectors of Σ [①③④] and Σ [❶❸❺], and they are of equal magnitude, the IMD_3 at both frequencies will be greatly reduced.

The above scenario is realized in Figure 5. We introduce a phase shift (of +90°) to the envelope signal when it is injected back to the main amplifier. As a result, both envelope-dependent nonlinear current vectors move to align themselves ~180° opposite to the fixed IMD_3 components. The resultant IMD_3 vectors at both $2\omega_1 - \omega_2$ and $2\omega_2 - \omega_1$ frequencies are substantially reduced.

Since the envelope detector circuit is very low-power and operates at baseband, the distortion cancellation technique has good potential for achieving both high-linearity *and* high-efficiency to meet the stringent requirements for modern communication applications.

III. Comparison of Measurement and Simulation Results

A WCDMA RF amplifier incorporating the envelope detection circuit of Figure 2 has been fabricated in a 0.25μm SiGe BiCMOS process [6]. The chip measures 1.75 × 0.7mm² (including pads) as shown in Figure 6. The amplifier has 16.5dB gain with 4.5mA (with 2.7V supply) quiescent current consumption and an output P_{1dB} of 8.5 dBm. Figure 7 shows the measured output spectrum at 0.5dBm (single-

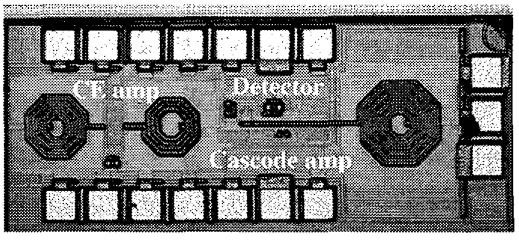

Figure 6. Microphotograph of the WCDMA RF amplifier.

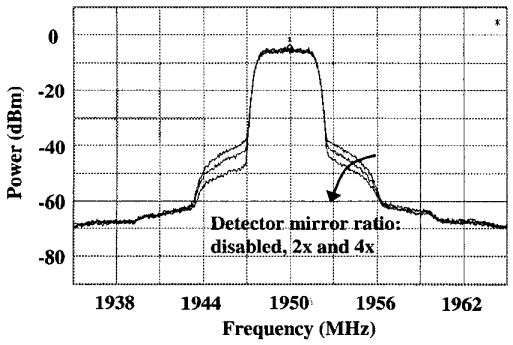

Figure 7. Measured RF amplifier output spectrum. While the envelope detector circuit improves the ACPR, spectral asymmetry is observed

ended) output power. The adjacent channel regrowth at 5MHz offset is caused by the 3rd-order IMD. It is reduced when the detector circuit is enabled. The adjacent channel power ratio (ACPR) is improved by 6dB to -43dBc.

As is evident in Figure 7, the ACPR improvement due to the detector circuit is *asymmetrical*. Better ACPR results are observed at the lower-side of the channel. This asymmetry is mainly caused by the envelope signal injection as explained in the previous Section. Figure 8 presents the measured amplifier 3rd-order intermodulation distortion results. Two sinusoidal signals at 1.9475 and 1.9525GHz are applied. The test is conducted for a wide range of input powers up to the input 1dB compression point of -8dBm. The figure shows the measured IMD_3 improvement when the envelope detector is enabled. The measured data are compared to the Volterra series calculations, and excellent agreement is obtained.

The effect of the phase of the envelope signal on intermodulation distortion is shown in Figure 9. The circuit of Figure 6 was simulated at the maximum power level, and an envelope signal of fixed amplitude and arbitrary phase is injected. The two-tone simulation results, together with the theoretical predictions, are shown in Figure 9, and excellent

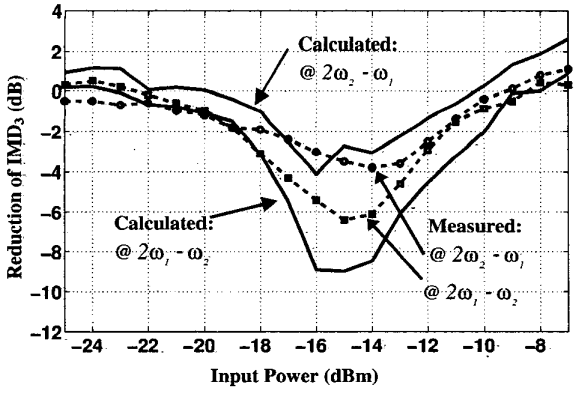

Figure 8. IMD_3 reduction versus input when the envelope detector is enabled. Good agreement is observed between the calculation and measured results, thus confirming the Volterra series analysis.

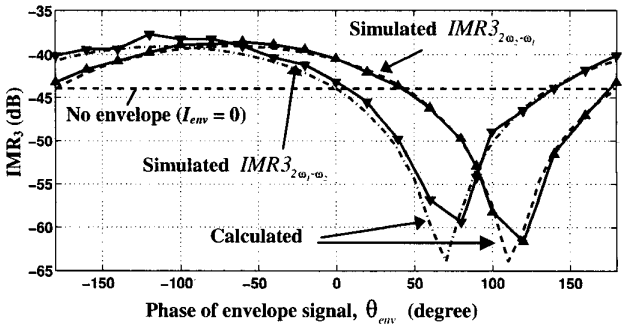

Figure 9. Comparison between calculation and simulation of IMD asymmetry with varying envelope injection phase. Maximum IMR3 cancellation is achieved when the envelope signal is injected with the optimal phase relative to the RF inputs

agreement is observed. The simulation verifies our intuition that optimal IMD cancellation will result at a particular envelope signal amplitude and phase angle. In this case, IMD at $2\omega_2 - \omega_1$ and $2\omega_1 - \omega_2$ show simultaneous improvement of 8dB.

IV. Summary

By making use of an envelope detector and feedback network that is compact and low-power, the linearity improvement technique described in this work is uniquely suitable for the design of high-linearity high-efficiency RF amplifiers. The distortion behavior was rigorously studied by Volterra series analysis. Very good agreement is observed between the theory, the simulated results, and the measured results.

References

[1] V. Leung, L. Larson, and P. Gudem, "Digital-IF WCDMA handset transmitter IC in 0.25um SiGe BiCMOS," *ISSCC Dig. Tech. Papers*, pp. 182-183, Feb. 2004.

[2] E. Taniguchi, K. Maeda, T. Ikushima, K. Sadahiro, K. Itoh, N. Suematsu, and T. Takgai, "Dual bias feed SiGe HBT low noise linear amplifier," *IEEE MTT-S Int. Microwave Symp. Dig.*, pp. 285-288, May 2001.

[3] *TS 25.101 (V5.3.0)*, 3GPP Standard, 2002.

[4] P. Wambacq and W. Sansen, *Distortion Analysis of Analog Integrated Circuits*, Kluwer Academic Publishers, pp. 137-156, 1998.

[5] S. A. Maas, *Nonlinear Microwave Circuits*, Norwood, MA: Artech House, pp. 190-207, 1998.

[6] IBM 6HP BiCMOS process, http://www-3.ibm.com/chips/techlib/techlib.nsf/products/BiCMOS_6HP

Appendix

The $D(\omega)$ expression can be written as:

$$D(\omega) = 1 - \omega^2 (C_\pi C_\mu Z_E Z_L + C_\pi C_\mu Z_E Z_S + C_\pi C_\mu Z_L Z_S) + g_m Z_E + j\omega [C_\pi Z_E + C_\mu Z_L + C_\pi Z_S + C_\mu Z_S + C_\mu g_m (Z_E Z_L + Z_E Z_S + Z_L Z_S)] \quad (13)$$